RSC Advances

PAPER

View Article Online
View Journal | View Issue

Cite this: *RSC Adv.*, 2020, **10**, 7619

PAMPS-*graft*-$Ni_3Si_2O_5(OH)_4$ multiwalled nanotubes as a novel nano-sorbent for the effective removal of Pb(II) ions†

Chunmei Xiao *[ab] and Jianming Lin[a]

The existence of Pb(II) ions in water systems poses significant potential hazards to public health and the environment. In the present study, poly(2-acrylamido-2-methylpropanesulfonic acid) (PAMPS) brush-modified $Ni_3Si_2O_5(OH)_4$ nanotubes were prepared, and their adsorption efficiency against the Pb(II) ions was investigated. The characterization results of FTIR spectroscopy, TGA, TEM, and XPS indicated the successful grafting of PAMPS on the surface of free $Ni_3Si_2O_5(OH)_4$ NTs, and the prepared PAMPS-*g*-$Ni_3Si_2O_5(OH)_4$ NTs exhibited a 6–8 nm grafting layer, which could provide abundant binding sites for metal adsorption. During the Pb(II) removal process, a pH-dependent adsorption behavior was observed, and the adsorption processes fitted well with the pseudo-second-order kinetic model and the Langmuir isotherm model. Compared with unmodified $Ni_3Si_2O_5(OH)_4$, the PAMPS-*g*-$Ni_3Si_2O_5(OH)_4$ NTs exhibited obviously faster adsorption of Pb(II) and higher equilibrium adsorption capacity for the removal of Pb(II). The maximum adsorption capacity calculated *via* the Langmuir isotherm model was 0.653 mmol g^{-1} (135.3 mg g^{-1}) at 298 K. In a metal coexisting system, the total adsorption capacity of the NTs was increased; this indicated the potential of the proposed NTs in the removal of Pb(II) from metal coexisting wastewater. This study showed the significant potential of PAMPS-*g*-$Ni_3Si_2O_5(OH)_4$ NTs in the effective removal of Pb(II).

Received 27th December 2019
Accepted 3rd February 2020

DOI: 10.1039/c9ra10971d

rsc.li/rsc-advances

1. Introduction

With the rapid development of social modernization, wastewater containing heavy metal ions is produced mainly from the metallurgy, tanning, battery and chemical manufacturing industries, which is causing a negative effect on the environment and human health.[1–3] Pb(II), ranked second in the list of prioritized hazardous substances issued by the US Agency for toxic substances and Disease Registry, has attracted significant concern as it can cause encephalopathy,[4] hepatitis,[5] nephritic syndrome and high blood pressure[6] even at low concentrations. In recent years, many technologies, such as chemical precipitation, electrodeposition, ion exchange, coagulation and adsorption, have been applied to remove Pb(II) from wastewater.[7–11] Among them, adsorption is regarded as the most effective method due to its low cost, ease of operation, flexibility, simplicity of design and environmental friendliness.[12–14]

Various adsorbents, including biomass, polymers, activated carbons and minerals, have been applied to remove Pb(II) from contaminated wastewater.[14–17] Moreover, it has been observed that these adsorbents require further modifications to increase the number of active binding sites and make them readily available for adsorption.[18,19] Although some of the above-mentioned adsorbents are able to remove Pb(II) from contaminated wastewater, high cost is still the main concern or disadvantage of these adsorbents in practical applications. Most of the inorganic minerals are limited by the drawbacks of costly regeneration, low adsorption capacity, poor selectivity and diversity of product structure and composition; however, some of them are still applied. Thus, an alternative adsorbent with high adsorption capacity and selectivity and rapid regeneration rate is urgently required to remove the Pb(II) ions from contaminated wastewater.

Nano-adsorbents not only work rapidly, but also have significant pollutant-binding capacities.[20–22] Unfortunately, unmodified nanomaterials are prone to agglomeration due to their several modes of interactions and consequently, their adsorption capacity and selectivity would be significantly reduced or lost. Thus, the modification of nanomaterials plays a key role in facilitating their stability. Many studies have been conducted on the modification of nanomaterials, such as nano-magnetic iron oxides,[23] nano-alumina,[24] hydroxyapatite nanoparticles,[25] and carbon nanotubes,[26] and their application in the

[a]College of Materials Science & Engineering, Huaqiao University, 361021, China. E-mail: chmxiao@qztc.edu.cn
[b]College of Chemical Engineering and Materials, Quanzhou Normal University, Quanzhou, 362002, China

† Electronic supplementary information (ESI) available. See DOI: 10.1039/c9ra10971d

treatment of heavy metals. Among them, silicate nanomaterials, especially silicate nanotubes (NTs), are considered as promising candidates as they remain well-dispersed and stable in aqueous solutions due to the negative charge and abundant silanol groups on their surfaces.[27–29] Some studies have reported the application of silicate NTs in metal removal such as silicate–titanate nanotubes in hydrogel exhibit efficient removal of Cd(II)[30] and PMAA-modified silicate nanotubes exhibit effective removal of Cu(II),[18] indicating the potential application prospect of silicate NTs. In addition, the molecular chain of polymers contains one or more electron donor atoms, such as N, S, O, and P, that can form coordinate bonds with most of the toxic heavy metals; thus, these polymers can be used to enrich or separate heavy metal ions by adsorption, chelation and ion exchange. Several researchers have reported that 2-acrylamido-2-methylpropanesulfonic acid (AMPS)-modified adsorbents exhibit high isoelectric point and good adsorption ability for metal ions in wastewater.[31–33] Some studies have reported that NTs can be modified by vinyl monomer or polymers including siloxane-poly(L-lactic acid)-vaterite[34] and poly(methacrylic acid).[18] However, no studies have been reported on the modification of silicate NTs by PAMPS. Thus, the assumption that PAMPS-modified silicate NTs will be highly efficient in the removal of Pb(II) from water is hypothetical.

Herein, we report the fabrication of a novel adsorbent by grafting AMPS onto nickel silicate NTs. As schematically shown in Fig. 1, an alkyl bromide-containing ATRP initiator was first immobilized on $Ni_3Si_2O_5(OH)_4$ NTs *via* a trimethylamine (TEA)-catalyzed condensation reaction. Subsequently, the AMPS polymer brushes were grafted onto the $Ni_3Si_2O_5(OH)_4$–NH surface (PAMPS-*g*-$Ni_3Si_2O_5(OH)_4$) *via* the ATRP method. The superiority of the PAMPS-*g*-$Ni_3Si_2O_5(OH)_4$ NTs is expected to not only significantly increase the number of adsorption sites and thus increase the uptake capacity of Pb(II) ions, but also facilitate the rapid regeneration of these NTs for recycling. The $Ni_3Si_2O_5(OH)_4$ and PAMPS-*g*-$Ni_3Si_2O_5(OH)_4$ NTs were characterized by Fourier transform infrared (FTIR) spectroscopy, X-ray photoelectron spectroscopy (XPS), thermogravimetric analysis (TGA), transmission electron microscopy (TEM), and scanning electron microscopy (SEM). Batch adsorption experiments were conducted to investigate the effect of solution pH on the adsorption capacity of Pb(II) ions, adsorption kinetics, adsorption isotherms and desorption of Pb(II) ions from the surfaces of the PAMPS-*g*-$Ni_3Si_2O_5(OH)_4$ NTs. Moreover, a hypothetical adsorption mechanism was proposed to account for the specific interactions between bonding sites and Pb(II) ions.

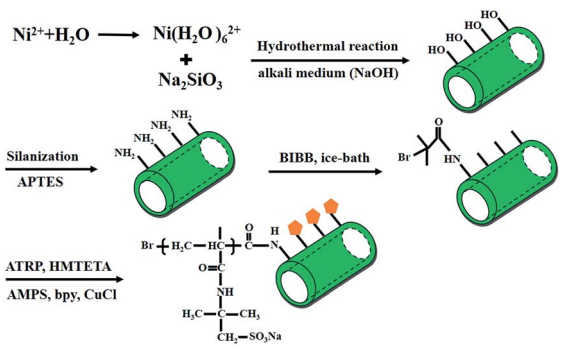

Fig. 1 Schematic illustration of the preparation of PAMPS-*g*-$Ni_3Si_2O_5(OH)_4$ nanotubes. The introduction of alkyl bromide-containing ATRP initiator on the surface of $Ni_3Si_2O_5(OH)_4$ NTs *via* trimethylamine (TEA)-catalyzed condensation reaction, and the grafting of AMPS polymer brushes on the surface of $Ni_3Si_2O_5(OH)_4$-NH_2 *via* ATRP method to prepare the PAMPS-*g*-$Ni_3Si_2O_5(OH)_4$ NTs.

2. Materials and methods

2.1. Materials

2-Acrylamido-2-methylpropanesulfonic acid (AMPS, >99%), triethylamine (TEA, >99%), methylbenzene and ethanol were purchased from Kelong Co., Ltd. (Chengdu, China). 3-Aminopropyltriethoxysilane (APTES, >96%) and 2-bromoisobutyryl bromide (BIBB, >98%) were purchased from Aladdin Industrial Co. (Shanghai, China). 1,1,4,7,10,10-Hexamethyltriethylenetetramine (HMDETA, >97%) was purchased from best-reagent Chemical Reagent Co. (Chengdu, China). Cuprous chloride, cupric chloride and Pb(II) ion standard solution (1000 mg L^{-1}) were purchased from Sigma-Aldrich Chemical Co. (St. Louis, MO, USA). All chemical reagents and solvents were of analytical grade and used without further purification. Deionized water used in the following experiments was purified using an ultrapure reverse osmosis system (Chengdu Ultrapure Technology Co. China).

2.2. Synthesis of PAMPS-*g*-$Ni_3Si_2O_5(OH)_4$ NTs

The preparation protocol for PAMPS-*g*-$Ni_3Si_2O_5(OH)_4$ NTs included four main steps. In the first step, the $Ni_3Si_2O_5(OH)_4$ NTs were prepared by a hydrothermal reaction method as previously reported.[35] In the second step, the $Ni_3Si_2O_5(OH)_4$–NH_2 NTs were prepared by reacting 0.2 g of $Ni_3Si_2O_5(OH)_4$ with 0.1 mL of APTES in 15 mL of methylbenzene under ultrasonic conditions. The suspension was refluxed for 24 h at 95 °C; then, the as-prepared $Ni_3Si_2O_5(OH)_4$–NH_2 NTs were rinsed several times with ethanol and deionized water alternately and dried for 12 h at 40 °C in a vacuum oven. In the third step, surface bromination of the $Ni_3Si_2O_5(OH)_4$–NH_2 NTs with BIBB was performed. Approximately 0.2 g of $Ni_3Si_2O_5(OH)_4$–NH_2 NTs was dispersed in a mixture of 15 mL methylbenzene, 0.3 mL of TEA and 0.1 mL of BIBB, and the mixture was refluxed for 24 h at 25 °C. The $Ni_3Si_2O_5(OH)_4$–Br NTs were rinsed several times with ethanol and deionized water alternately and dried for 12 h at 40 °C in a vacuum oven. In the fourth step, the immobilization of PAMPS on the formed $Ni_3Si_2O_5(OH)_4$–Br NTs was achieved through the SI-ATRP described in our previous study. Typically, 0.2 g of $Ni_3Si_2O_5(OH)_4$–Br NTs was dispersed in 4 mL of AMPS solutions (pH = 7.5) under a N_2 atmosphere, and then, $CuCl_2$, HMTETA and CuCl were added in turn (n[AMPS] : n[CuCl] : n[$CuCl_2$] : n[HMTETA] = 50 : 1.0 : 0.1 : 1) and reacted at 50 °C for 8 hours. Finally, the obtained products were rinsed several times with ethanol and deionized water alternately to remove the oligomers and residual copper and then dried at 40 °C for 12 h.

2.3. Characterization of the PAMPS-*g*-$Ni_3Si_2O_5(OH)_4$ NTs

The obtained PAMPS-*g*-$Ni_3Si_2O_5(OH)_4$ NTs were characterized to confirm their structural features. The morphologies of PAMPS-*g*-$Ni_3Si_2O_5(OH)_4$ NTs were observed using the Tecnai G2 F20 S-TWIN field-emission transmission electron microscope (FE-TEM, FEI, USA) equipped with an energy dispersive X-ray spectrometer (EDS, JEOL, Japan). The FTIR spectrum was obtained using a frontier FTIR spectrometer (PerkinElmer, USA) with KBr disks in the wavenumber range of 600–4000 cm^{-1}. XPS measurements were conducted using the Kratos AXIS Ultra DLD spectrometer (Kratos Analytical, UK) under monochromatized AlKα X-ray radiation (1486.6 eV). The organic loading in the PAMPS-*g*-$Ni_3Si_2O_5(OH)_4$ NTs was measured by TGA performed using the TGA/DSC 2 thermogravimetric analyzer (Mettler Toledo, Switzerland) at the heating rate of 20 °C min^{-1} from 30 °C to 700 °C under a nitrogen atmosphere.

2.4. Batch adsorption experiments

2.4.1. Effect of solution pH. The effect of pH on Pb(II) adsorption was studied after adding 50 mg of PAMPS-*g*-$Ni_3Si_2O_5(OH)_4$ NTs to 100 mL of a Pb(II) solution (0.24 mmol L^{-1}) in the pH range of 1.0–6.0. These flasks were shaken in a thermostatic shaker at 298 K for 120 min. The Pb(II) concentrations of each sample before and after adsorption were determined by an AA240 atomic absorption spectrometer (Varian, USA). The Pb(II) removal rate (R) and adsorption capacity (q_e, mg g^{-1}) were calculated according to eqn (1) and (2), respectively.

$$R = \frac{c_0 - c_e}{c_0} \times 100\% \quad (1)$$

$$q_e = \frac{(c_0 - c_e) \times V}{m} \quad (2)$$

where q_e (mg g^{-1}) is the amount of Pb(II) adsorbed per gram of PAMPS-*g*-$Ni_3Si_2O_5(OH)_4$ NTs at equilibrium, c_0 is the initial Pb(II) concentration (mg L^{-1}), c_e is the residual Pb(II) concentration (mg L^{-1}), V stands for the volume of the solution (L), and m is the mass of the adsorbent (g).

2.4.2. Adsorption kinetics. The adsorption kinetics experiments were carried out in 100 mL of a 0.24 mmol L^{-1} Pb(II) solution with 50 mg of PAMPS-*g*-$Ni_3Si_2O_5(OH)_4$ NTs. The pH value of the solutions was adjusted to 5.0, and the adsorption process was conducted at 298 K for the time intervals of 2, 5, 8, 10, 15, 30, 60, 90, and 120 min. The concentration of Pb(II) was analyzed at regular intervals during the adsorption process.

2.4.3. Adsorption isotherms. Isothermal adsorption experiments were conducted in 100 mL of Pb(II) solution, where the initial concentrations of Pb(II) ranged from 0.097 mmol L^{-1} to 0.58 mmol L^{-1} and the dose of PAMPS-*g*-$Ni_3Si_2O_5(OH)_4$ NTs was 50 mg. The pH value of the solutions was adjusted to 5.0, and the adsorption process was conducted at 298 K successively for 120 min. The adsorption capacity at equilibrium was calculated according to the mass balance of Pb(II) before and after adsorption.

2.4.4. Regeneration of the PAMPS-*g*-$Ni_3Si_2O_5(OH)_4$ NTs. For the examination of the desorption properties of adsorbent, 50 mg of PAMPS-*g*-$Ni_3Si_2O_5(OH)_4$ NTs was added to 100 mL of the Pb(II) solution with the initial concentration and pH of 0.24 mmol L^{-1} and 5.0, respectively. The mixtures were then placed in a shaking bath at 298 K and 150 rpm for 120 min. The adsorbent was separated from the solution, washed with distilled water, and used in the desorption tests. For the regeneration tests, the saturated adsorbent was stirred in 20 mL of HCl solution (0.1 mol L^{-1}) at 298 K and 150 rpm for 60 min. Then, the adsorbents were washed with distilled water and dried in an oven before the re-adsorption tests. The removal rates in each cycle were measured.

3. Results and discussion

3.1. Characterization of PAMPS-*g*-$Ni_3Si_2O_5(OH)_4$ NTs

The prepared PAMPS-*g*-$Ni_3Si_2O_5(OH)_4$ NTs were obtained and dried for structural characterization. The FTIR spectra (Fig. 2A) could preliminarily confirm the formation of the modified NTs. In the spectrum of $Ni_3Si_2O_5(OH)_4$ NTs (Fig. 2A(a) and S1†), the peak at 3652 cm^{-1} was attributed to the stretching vibrations of Ni–OH and the peak at 3450 cm^{-1} corresponded to the stretching vibrations of the hydroxyl group. Typical asymmetric stretching vibrations were observed at 1070 cm^{-1} and 980 cm^{-1}, which demonstrated the presence of Si–O and Si–O–Si, respectively. Fig. 2A(b) and (c) exhibit a new peak at 1720 cm^{-1}, corresponding to the O=C–N group, indicating that the surface of the $Ni_3Si_2O_5(OH)_4$ NTs has been successfully amidated. Fig. 2A(d) and (e) show the spectra of the final PAMPS-*g*-$Ni_3Si_2O_5(OH)_4$ product obtained at different reaction times. In their spectra, peaks at 1043 cm^{-1} and 1201 cm^{-1}, which corresponded to the features of the S=O group, were observed, indicating the existence of sulfonic groups. In addition, the

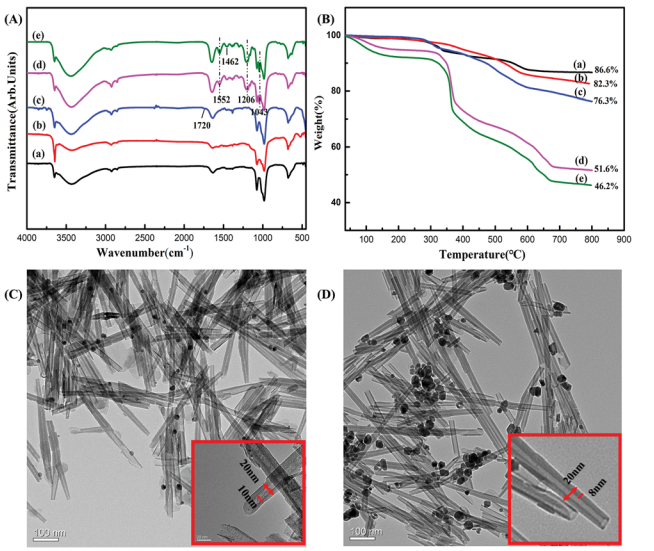

Fig. 2 (A) FTIR spectra and (B) TG curves of (a) $Ni_3Si_2O_5(OH)_4$, (b) $Ni_3Si_2O_5(OH)_4$–NH_2, (c) $Ni_3Si_2O_5(OH)_4$–Br, (d) PAMPS-*g*-$Ni_3Si_2O_5(OH)_4$-1 prepared *via* a 2 h ATRP reaction, and (e) PAMPS-*g*-$Ni_3Si_2O_5(OH)_4$-2 prepared *via* an 8 h ATRP reaction. TEM images of (C) $Ni_3Si_2O_5(OH)_4$ and (D) PAMPS-*g*-$Ni_3Si_2O_5(OH)_4$ NTs.

bending vibration absorption bands I, II, and III of the N–H of acrylamide were observed at 1680 cm^{-1}, 1552 cm^{-1}, and 1300 cm^{-1}, respectively. The results indicated that the PAMPS polymer brushes were successfully bound on the surface of the $Ni_3Si_2O_5(OH)_4$ NTs. The TG curves of the NTs obtained before and after modification are shown in Fig. 2B. Free $Ni_3Si_2O_5(OH)_4$ NTs exhibited three mass loss stages and finally remained stable when heated to 600 °C. The mass loss stage from 60 °C to 180 °C corresponded to the loss of physically adsorbed water; the stage from 250 °C to 500 °C indicated the condensation and dehydration of the hydroxyl groups on the surface of NTs, and the stage between 500 °C and 600 °C corresponded to the further decomposition of hydroxyl groups. In the spectrum of $Ni_3Si_2O_5(OH)_4$–ABr (Fig. 2B(c)), the mass loss rates in the 300 °C–500 °C range were obviously increased; this possibly resulted from the decomposition of the introduced amide groups and Br. However, for the final product PAMPS-*g*-$Ni_3Si_2O_5(OH)_4$ (Fig. 2B(d) and (e)), the mass loss in the range from 250 °C to 500 °C was significantly increased, which corresponded to the condensation of the successfully grafted PAMPS.

On the other hand, the mass loss of the product obtained after an 8 h reaction was significantly higher than that of the product obtained after a 2 h reaction; this indicated a positive correlation between the PAMPS grafting rate and reaction time. This phenomena could also be observed from the DTA curves (Fig. S2†). Only slightly endothermic phenomena were observed before the grafting of PAMPS. However, a significantly enhanced endothermic rate was detected after the grafting of PAMPS, which further indicated the successful grafting of PAMPS. Moreover, the endothermic rate in the stage from 250 °C to 500 °C of the product obtained after reaction for 8 h was obviously higher than that of the product obtained after reaction for 2 h; this also indicated that prolonging the reaction time was helpful for PAMPS grafting. Uniform size and excellent dispersion were observed in the surface morphology of PAMPS-*g*-$Ni_3Si_2O_5(OH)_4$ NTs. Compared with free NTs, the modified NTs exhibited a grafting layer with a thickness of about 6–8 nm (Fig. 2D), which could provide abundant binding sites for metal adsorption. In the C 1s XPS spectrum of PAMPS-*g*-$Ni_3Si_2O_5(OH)_4$ NTs (Fig. 3), the peaks of C–H (284.6 eV), C–N (285.2 eV), C–S (286.6 eV), and O=C–NH (287.0 eV) were observed. However, a new signal was observed at 168.0 eV that corresponded to S 2p, and the intensity of the N 1s peak at 400.1 eV was markedly enhanced than that in the case of the intermediate product (Fig. S3†). Thus, the abovementioned characterization indicated that the PAMPS chain was successfully grafted onto the surface of free $Ni_3Si_2O_5(OH)_4$ NTs.

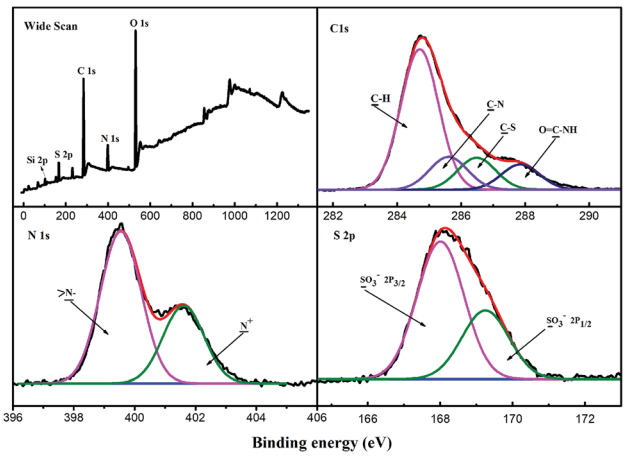

Fig. 3 XPS spectra of the prepared PAMPS-*g*-$Ni_3Si_2O_5(OH)_4$ NTs.

3.2. Effect of initial pH on Pb(II) adsorption

Solution pH is an important parameter during the adsorption process due to its strong influence on the surface characteristics of the adsorbent and the speciation of heavy metal ions in solution.[36,37] The surface charges of $Ni_3Si_2O_5(OH)_4$ and PAMPS-*g*-$Ni_3Si_2O_5(OH)_4$ NTs were examined by zeta potential measurement in the pH range 1.0–12.0 (Fig. S4†). The pH_{zpc} (pH zero-point charge) values of $Ni_3Si_2O_5(OH)_4$ and PAMPS-*g*-$Ni_3Si_2O_5(OH)_4$ NTs were about 4.2 and 2.3, respectively. For $Ni_3Si_2O_5(OH)_4$, the positive surface potential is attributed to the protonation of the hydroxyl groups from Si–OH and Ni–OH. After the introduction of AMPS, the pH_{zpc} value of the PAMPS-*g*-$Ni_3Si_2O_5(OH)_4$ NTs decreased due to the protonation of the sulfonic acid group, indicating the successful grafting of AMPS. With an increase in the solution pH, the zeta potential gradually decreased and became negative. This result should be ascribed to the deprotonation of corresponding groups and favors cation adsorption by electrostatic interaction.

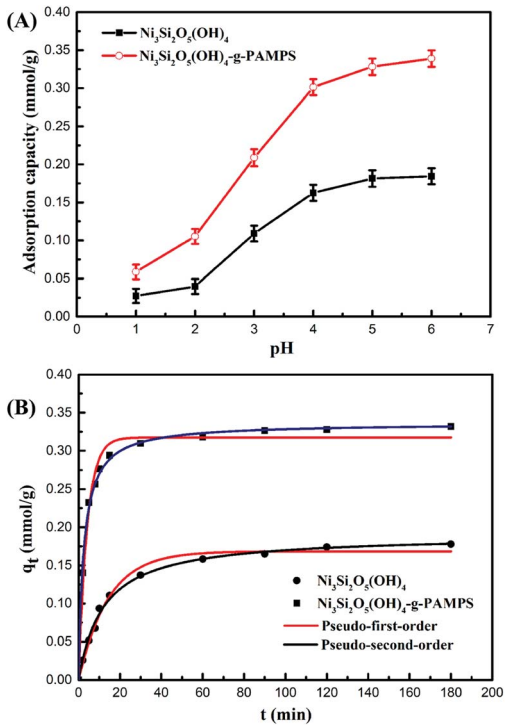

Fig. 4 (A) The effect of pH on the removal of Pb(II) using PAMPS-*g*-$Ni_3Si_2O_5(OH)_4$ NTs; (B) fitting curves for Pb(II) adsorption on PAMPS-*g*-$Ni_3Si_2O_5(OH)_4$ NTs obtained using pseudo-first-order (PFO) and pseudo-second-order (PSO) kinetic models.

Fig. 4A shows the effect of initial solution pH on the adsorption of Pb(II) on $Ni_3Si_2O_5(OH)_4$ and PAMPS-*g*-$Ni_3Si_2O_5(OH)_4$ NTs in the pH range of 1.0–6.0. It is obvious that the adsorption of Pb(II) on the $Ni_3Si_2O_5(OH)_4$ and PAMPS-*g*-$Ni_3Si_2O_5(OH)_4$ NTs increases with an increase in the solution pH due to complexation between Pb(II) and functional groups, such as hydroxyl and sulfonic acid groups, on the surface of adsorbents. At lower pH values, excess H^+ protonates the material and the surface charge of the material becomes positive, which hinders the electrostatic attraction between the material and the Pb(II) ion. The maximum adsorption capacity of PAMPS-*g*-$Ni_3Si_2O_5(OH)_4$ NTs (0.342 mmol g^{-1}) was higher than that of $Ni_3Si_2O_5(OH)_4$ (0.172 mmol g^{-1}); this indicated that the sulfonic acid group was the main adsorption site for Pb(II). As the pH values increased from 1.0 to 6.0, the functional group $-SO_3H$ was deprotonated to $-SO_3^-$, which could form a complex with Pb(II). These results indicated that the dominant Pb(II) adsorption sites on the PAMPS-*g*-$Ni_3Si_2O_5(OH)_4$ NTs were the deprotonated sulfonic acid groups in the AMPS structure. Based on the results of zeta potential and Pb(II) adsorption at different pH values, the pH value of 5.0 was found to the optimum value for Pb(II) removal by the PAMPS-*g*-$Ni_3Si_2O_5(OH)_4$ NTs.

3.3. Adsorption kinetics

Adsorption kinetics, which concerns the mass transfer of the adsorption process, is an important consideration in the practical application of potential adsorbents.[38–40] Fig. 4B illustrates the adsorption kinetic data of Pb(II) adsorption onto $Ni_3Si_2O_5(OH)_4$ and PAMPS-*g*-$Ni_3Si_2O_5(OH)_4$ NTs. In the first 20 min, the adsorption capacity of PAMPS-*g*-$Ni_3Si_2O_5(OH)_4$ NTs for Pb(II) reached 0.295 mmol g^{-1}, and the adsorption equilibrium was reached at 60 min with an adsorption capacity of 0.33 mmol g^{-1}. However, the adsorption capacity of $Ni_3Si_2O_5(OH)_4$ for Pb(II) was only 0.125 mmol g^{-1} in the first 20 min. The adsorption rate of Pb(II) in the case of PAMPS-*g*-$Ni_3Si_2O_5(OH)_4$ NTs was significantly faster than that in the case of $Ni_3Si_2O_5(OH)_4$. It can be observed that the adsorption rate of Pb(II) is very fast; this is consistent with the previously reported fact that the fast adsorption rate in the case of nanostructures is due to the short diffusion path and low diffusion resistance of nanostructures. This phenomenon indicated that the PAMPS-*g*-$Ni_3Si_2O_5(OH)_4$ NTs provided more adsorption sites due to the introduction of the sulfonic acid group.

The pseudo-first-order and pseudo-second-order kinetic models were further employed to obtain the adsorption kinetic data, and their equations are expressed as follows:[41]

Pseudo-first-order:

$$\log(q_e - q_t) = \log q_e - \frac{k_1 \times t}{2.303} \quad (3)$$

Pseudo-second-order:

$$\frac{t}{q_t} = \frac{1}{k_2 \times q_e^2} + \frac{t}{q_e} \quad (4)$$

where q_t (mg g^{-1}) and q_e (mg g^{-1}) represent the amount of Pb(II) adsorbed at time t and at equilibrium time, respectively; k_1 (min^{-1}) and k_2 (g mg^{-1} min^{-1}) represent the rate constants of the pseudo-first-order and pseudo-second-order kinetic models, respectively.

The pseudo-second-order kinetic model was more suitable to fit the experimental data according to the correlation coefficients (R^2) of the pseudo-first-order and pseudo-second-order. (Table 1). The calculated equilibrium adsorption capacities q_e were 39.45 mg g^{-1} and 69.68 mg g^{-1} for $Ni_3Si_2O_5(OH)_4$ and PAMPS-*g*-$Ni_3Si_2O_5(OH)_4$ NTs, respectively. These values were extremely close to the experimentally determined adsorption capacities (0.1904 and 0.3363 mmol g^{-1}). On the other hand, the gained adsorption capacity (69.68 mg g^{-1}) was higher than those of the several previously reported materials such as apricot stone activated carbon (21.38 mg g^{-1}),[42] pine cone activated carbon (27.53 mg g^{-1}),[43] and silica-modified calcium alginate–xanthan gum (18.9 mg g^{-1}).[44]

3.4. Adsorption isotherms

Adsorption isotherms are widely used methods to evaluate the distribution of pollutants between the solid and liquid phase, which are beneficial to understand the nature of adsorption.[45] In order to investigate the adsorption characteristic of PAMPS-*g*-$Ni_3Si_2O_5(OH)_4$ NTs against Pb(II), two commonly used models, *i.e.* Langmuir and Freundlich models, were employed to describe the adsorption process. The two models are presented as follows:[46]

$$q_e = K_L q_{max} C_e/(1 + K_L C_e) \quad (5)$$

$$q_e = K_F C_e^{1/n} \quad (6)$$

where q_e (mmol g^{-1}) is the pollutant uptake at equilibrium, q_{max} (mmol g^{-1}) is the maximum adsorption capacity, C_e (mmol L^{-1}) is the residual pollutant concentration, K_L (L $mmol^{-1}$) is the Langmuir binding constant, K_F is the Freundlich constant related to adsorption capacity, and n is a constant that describes the adsorption intensity.

The fitting curves of the two isotherm models at 298.15 K, 308.15 K, 318.15 K, and 328.15 K are illustrated in Fig. 5, and the corresponding equilibrium parameters are listed in Table 2. It can be observed that the adsorption capacity of the PAMPS-*g*-$Ni_3Si_2O_5(OH)_4$ NTs exhibits a positive correlation with the Pb(II) initial concentration as well as temperature. For all the systems considered in this study, the fitting degree of the Langmuir model was obviously better than that of the Freundlich model; this indicated that Langmuir isotherm could acquire more accurate parameters and was more suitable to evaluate the thermodynamic process. On the other hand, the Langmuir model assumes that the adsorption process only takes place on the outer surface of the adsorbent, the surface of the adsorbent is uniform, and there is no interaction between the adsorbed substances in the adsorption process. Thus, it could be speculated that the grafted PAMPS was possibly uniformly distributed on the surface of the NTs. The calculated maximum adsorption capacities (q_m) of Pb(II) were 0.653, 0.672, 0.688, and 0.694 mmol g^{-1} at 298, 308, 318, and 328 K, respectively. These

Table 1 Parameters of kinetic models predicting the experimental data for the adsorption of Pb(II) ions on the $Ni_3Si_2O_5(OH)_4$ and PAMPS-*g*-$Ni_3Si_2O_5(OH)_4$ NTs

		Model parameters				
Samples	Models	K_f (min^{-1})	K_s (g $mmol^{-1}$ min^{-1})	q_e (mmol g^{-1})	χ^2 ($\times10^{-5}$)	R^2
$Ni_3Si_2O_5(OH)_4$	PFO	0.070	—	0.1685	4.635	0.988
	PSO	—	0.4359	0.1904	2.002	0.995
PAMPS-*g*-$Ni_3Si_2O_5(OH)_4$	PFO	0.2434	—	0.3174	16.329	0.984
	PSO	—	1.2116	0.3363	2.998	0.997

high adsorption capacities possibly resulted from the nanostructure and the abundant binding sites.

The effect of temperature on the adsorption of Pb(II) by PAMPS-*g*-$Ni_3Si_2O_5(OH)_4$ NTs at 298, 308, 318 and 328 K is shown in Fig. 6. Thermodynamic parameters, including Gibbs free energy (ΔG), entropy change (ΔH) and enthalpy change (ΔS), were further used to study the thermal properties during the adsorption process, which were calculated according to the van't Hoff equations[47] as follows:

$$\Delta G = -RT \ln K \quad (7)$$

$$\ln K = -\frac{\Delta H}{RT} + \frac{\Delta S}{R} \quad (8)$$

where R is the ideal gas constant (8.314 J mol^{-1} K^{-1}), T is the temperature in Kelvin, and K (L mol^{-1}) is the adsorption equilibrium constant.

ΔH and ΔS were calculated from the slope and intercept of the linear plot according to $\ln K$ *versus* $1/T$ (Fig. 6), and the relative parameters are listed in Table 3. The positive ΔH and ΔS values show that the adsorption of Pb(II) by the PAMPS-*g*-$Ni_3Si_2O_5(OH)_4$ NTs is an endothermic and entropy-driven process. The negative values of ΔG illustrate that the adsorption of Pb(II) by the PAMPS-*g*-$Ni_3Si_2O_5(OH)_4$ NTs is spontaneous. The ΔG value decreased with an increase in temperature, indicating that the adsorption of Pb(II) by the PAMPS-*g*-$Ni_3Si_2O_5(OH)_4$ NTs was promoted at higher temperatures.

Table 2 The parameters of the Langmuir and Freundlich models for Pb(II) adsorption on PAMPS-*g*-$Ni_3Si_2O_5(OH)_4$ NTs at different temperatures

		Temperature (K)			
Models	Fitted parameters	298.15	308.15	318.15	328.15
Langmuir	q_{max} (mmol g^{-1})	0.653	0.672	0.688	0.694
	K_L (L $mmol^{-1}$)	12.239	14.842	18.324	26.341
	χ^2 ($\times10^{-4}$)	2.028	3.205	2.492	3.623
	R^2	0.993	0.990	0.993	0.991
Freundlich	K_F ($mmol^{1-1/n}$ $L^{1/n}$ g^{-1})	0.871	0.920	0.971	1.007
	n	2.419	2.546	2.670	2.950
	χ^2 ($\times10^{-3}$)	1.230	1.570	1.510	1.820
	R^2	0.957	0.952	0.958	0.956

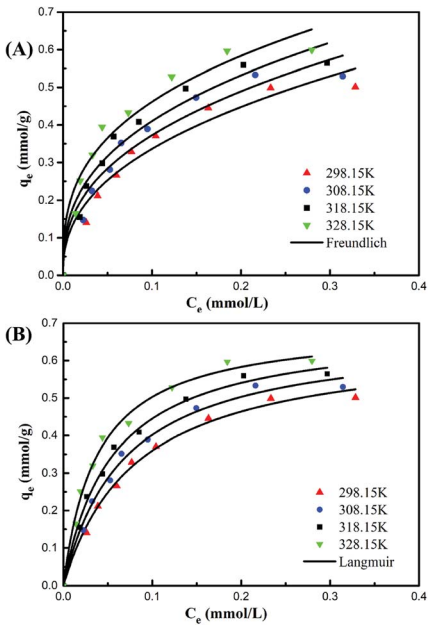

Fig. 5 Fitting curves of Pb(II) adsorption thermodynamics obtained using (A) Freundlich and (B) Langmuir isotherm models for the PAMPS-*g*-$Ni_3Si_2O_5(OH)_4$ NTs.

3.5. Possible mechanism of adsorption of Pb(II) on PAMPS-*g*-$Ni_3Si_2O_5(OH)_4$ NTs

The surface chemistry of the adsorbent before and after adsorption was studied by XPS using the Kratos Axis Ultra DLD X-ray photoelectron spectrometer to further investigate the

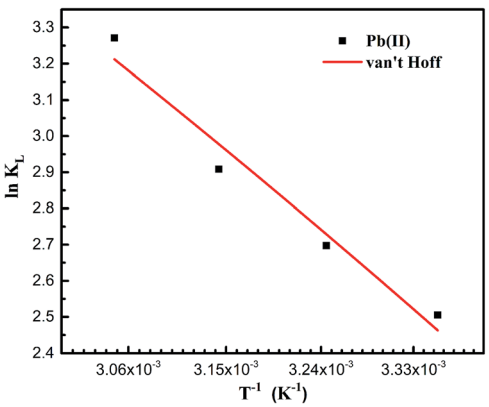

Fig. 6 van't Hoff fitting of the thermodynamic parameters at 298, 308, 318 and 328 K.

Table 3 Thermodynamic parameters for Pb(II) removal using the PAMPS-*g*-$Ni_3Si_2O_5(OH)_4$ NTs

Temperature (K)	ΔH^0 (kJ mol^{-1})	ΔS^0 (J mol^{-1})	ΔG^0 (kJ mol^{-1})
298.15	20.32	88.62	−6.102
308.15			−6.988
318.15			−7.874
328.15			−8.761

possible interactions. The XPS results are illustrated in Fig. 7. Compared with the spectra of the free PAMPS-*g*-$Ni_3Si_2O_5(OH)_4$ NTs shown in Fig. 3, new peaks of Pb 4f and Pb 4d were observed at 139.11 eV and 414.1 eV, respectively, in the total scans of the XPS spectra of the metals after adsorption (Fig. 7), which confirmed the successful adsorption of Pb(II) on the adsorbent. In the high-resolution spectra of C 1s, the intensities of the peaks corresponding to C–S and O=C–N were greatly decreased after the adsorption of Pb(II); this indicated the involvement of the sulfonic group and heteroatoms in the adsorption of metal ions. In the high-resolution spectra of O 1s, the area about 531.0 eV that correspond to the oxygen atoms from coordination system with metal was observed, indicating the formation of Pb–O. In addition, the spectrum of Pb 4f was composed of two peaks at 139.2 eV and 143.8 eV, corresponding to Pb $4f_{7/2}$ and Pb $4f_{5/2}$. Therefore, these phenomena indicated that the adsorption of Pb(II) on PAMPS-*g*-$Ni_3Si_2O_5(OH)_4$ NTs was mainly based on the interaction between the oxygen atom in the sulfonic group and metal ions.

3.6. Removal of co-existing metal ions

In an actual wastewater system, there are usually many coexisting pollutants. Therefore, it is of great significance to study the removal efficiency of coexisting pollutants. In the present study, the competition of Pb(II) with other metal ions, *i.e.* Cu(II) and Mg(II), was investigated through static adsorption experiment. As illustrated in Fig. 8A, these three metal ions could be adsorbed by the NTs based on the interaction between the metal ions and sulfonic adsorption sites. The adsorption capacity of the PAMPS-*g*-$Ni_3Si_2O_5(OH)_4$ NTs for Pb(II) was slightly lower than that of the free NTs, whereas the total adsorption capacity for the three metal ions was increased by about 17.2%. These phenomena indicated the perfect metal removal capacities of the PAMPS-*g*-$Ni_3Si_2O_5(OH)_4$ NTs. In addition, the removal efficiency of Pb(II) was obviously higher than those of Cu(II) and Mg(II), and the difference between the adsorption capacities was in agreement with the hard–soft–acid–base (HSAB) theory. The sulfonic group is handover base, Pb(II) and Cu(II) is boric acid, and Mg(II) is hard acid. Moreover, Pb(II) has a bigger ionic radius; thus, the coordination ability between the sulfonic group and the three metals exhibits the following order: Pb(II) > Cu(II) > Mg(II). The results demonstrate that the PAMPS-*g*-$Ni_3Si_2O_5(OH)_4$ NTs are an excellent adsorbent for the removal of coexisting metals from wastewater.

3.7. Desorption and regeneration abilities

The regeneration and reuse ability of a smart adsorbent is an important factor for its further application. The surface of the PAMPS-*g*-$Ni_3Si_2O_5(OH)_4$ NTs contains large amount of sulfonic groups, which can adsorb Pb(II) *via* electrostatic interaction. In the desorption process, the Pb(II)-bonded sulfonic groups could be reproduced through the ion exchange of Pb(II) by H^+. In this study, the NTs were regenerated using 0.1 M HCl followed by washing with deionized water. As shown in Fig. 8B, the removal

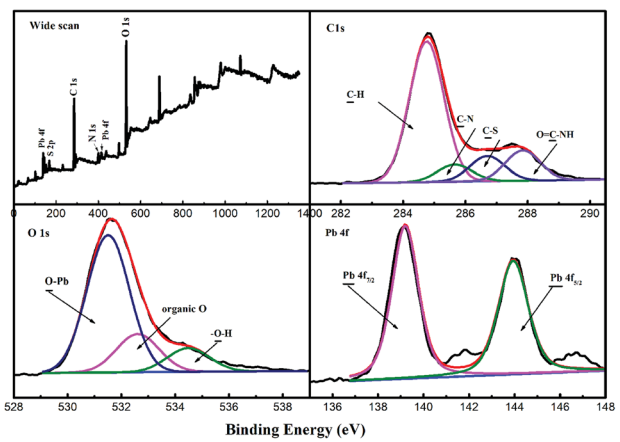

Fig. 7 XPS spectra of the PAMPS-*g*-$Ni_3Si_2O_5(OH)_4$ NTs after the adsorption of Pb(II).

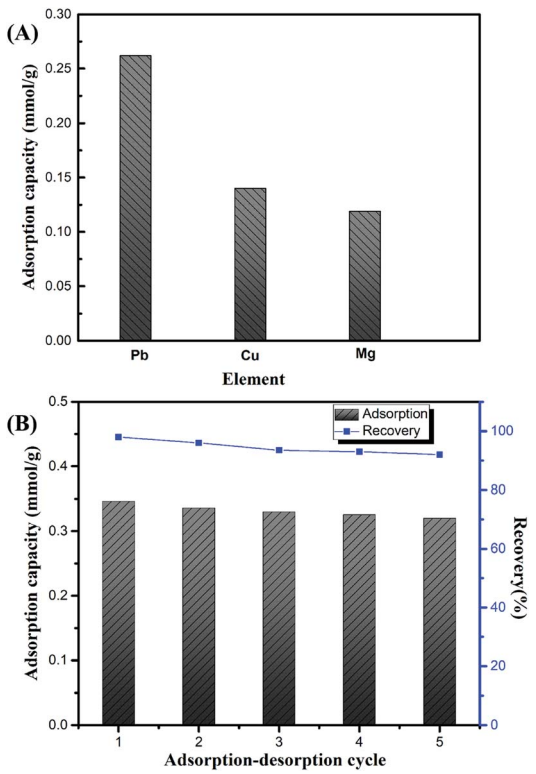

Fig. 8 (A) The adsorption capacities of PAMPS-*g*-$Ni_3Si_2O_5(OH)_4$ NTs against the Pb(II), Cu(II), and Mg(II) co-existing system, and (B) regeneration and recovery of the PAMPS-*g*-$Ni_3Si_2O_5(OH)_4$ NTs.

efficiency of the regenerated NTs was maintained at a high level (higher than 90%), and only a slight decrease was observed after three desorption/adsorption cycles. We speculated that the reduction resulted from the formation of a tiny amount of Pb(II) complex. Overall, the reuse phenomena indicate that the PAMPS-*g*-$Ni_3Si_2O_5(OH)_4$ NTs exhibit well regeneration ability after simple picking and rinsing and are a promising adsorbent.

4. Conclusions

In the present study, a novel adsorbent, PAMPS-*g*-$Ni_3Si_2O_5(OH)_4$ NTs, was fabricated *via* the grafting of PAMPS brushes onto the surface of nickel silicate NTs. The structure of the adsorbent was characterized by FTIR spectroscopy, TGA, TEM, and XPS. Batch adsorption studies indicated that the adsorption capacity of the PAMPS-*g*-$Ni_3Si_2O_5(OH)_4$ NTs was closely related to the pH value, and an optimized removal efficiency was achieved against Pb(II) at the pH value of 5.0. The adsorption kinetics study indicated that the pseudo-second-order kinetic model was highly suitable to fit the experimental data. The calculated equilibrium adsorption capacity q_e was 0.3363 mmol g^{-1} (69.68 mg g^{-1}) for PAMPS-*g*-$Ni_3Si_2O_5(OH)_4$ NTs, which was higher than 0.1904 mmol g^{-1} (39.45 mg g^{-1}) gained by free $Ni_3Si_2O_5(OH)_4$. The Langmuir-fitted maximum adsorption capacity of Pb(II) on PAMPS-*g*-$Ni_3Si_2O_5(OH)_4$ NTs was 0.653 mmol g^{-1} (135.3 mg g^{-1}) at 298 K. In addition, the PAMPS-*g*-$Ni_3Si_2O_5(OH)_4$ NTs adsorbent was highly efficient for the removal of coexisting metals from wastewater. The XPS results revealed that the possible adsorption mechanism for the removal of Pb(II) involved interaction between the oxygen atom of the sulfonic group and metal ions. Overall, the PAMPS-*g*-$Ni_3Si_2O_5(OH)_4$ NTs could be a promising candidate for the uptake of metal pollutants from water.

Conflicts of interest

There are no conflicts to declare.

Acknowledgements

The authors gratefully acknowledge Yu Zheng for their help in the preparation of free $Ni_3Si_2O_5(OH)_4$ NTs and ceshigo for the XPS testing service from "http://www.ceshigo.com".

References

1 A. O. W. Leung, N. S. Duzgoren-Aydin, K. C. Cheung and M. H. Wong, *Environ. Sci. Technol.*, 2008, **42**, 2674–2680.
2 Z. Y. Li, Z. W. Ma, T. J. van der Kuijp, Z. W. Yuan and L. Huang, *Sci. Total Environ.*, 2014, **468**, 843–853.
3 Y. M. Dai, D. Y. Liu, J. Q. Zou, S. Y. Wang and Y. Zhou, *RSC Adv.*, 2019, **9**, 9171–9179.
4 M. Moshtaghie, P. Malekpouri, M. Saeed-zadeh, M. Messripour and A. A. Moshtaghie, *Iran. J. Pharm. Res.*, 2013, **12**, 461–468.
5 G. D. Kamenov and B. L. Gulson, *Sci. Total Environ.*, 2014, **490**, 861–870.
6 V. Rapisarda, C. Ledda, M. Ferrante, M. Fiore, S. Cocuzza, M. Bracci and C. Fenga, *Toxicol. Ind. Health*, 2016, **32**, 1729–1736.
7 X. M. Ren, D. D. Shao, S. T. Yang, J. Hu, G. D. Sheng, X. L. Tan and X. K. Wang, *Chem. Eng. J.*, 2011, **170**, 170–177.
8 Z. Lin, X. L. Weng, G. Owens and Z. L. Chen, *J. Clean. Prod.*, 2020, **242**, 9.
9 X. Chen, S. Sun, X. Wang, J. Wen, Y. Wang, X. Cao, T. Yuan, S. Wang, Q. Shi and R. Sun, *Bioresour. Technol.*, 2019, 122297.
10 A. J. Bora and R. K. Dutta, *Journal of Water Process Engineering*, 2019, **31**, 9.
11 C. J. Madadrang, H. Y. Kim, G. H. Gao, N. Wang, J. Zhu, H. Feng, M. Gorring, M. L. Kasner and S. F. Hou, *ACS Appl. Mater. Interfaces*, 2012, **4**, 1186–1193.
12 M. Sprynskyy, B. Buszewski, A. P. Terzyk and J. Namiesnik, *J. Colloid Interface Sci.*, 2006, **304**, 21–28.
13 Y. L. Zhao, R. Y. Zhang, H. B. Liu, M. X. Li, T. H. Chen, D. Chen, X. H. Zou and R. L. Frost, *Chem. Eng. J.*, 2019, **375**, 10.
14 J. Gatabi, Y. Sarrafi, M. M. Lakouraj and M. Taghavi, *Chemosphere*, 2019, **240**, 124772.
15 L. N. M. Yabuki, A. A. Menegario, H. Gemeiner, A. Rolisola, D. Gastmans and P. N. Williams, *Talanta*, 2019, **205**, 9.
16 W. R. Lim, S. W. Kim, C. H. Lee, E. K. Choi, M. H. Oh, S. N. Seo, H. J. Park and S. Y. Hamm, *Sci. Rep.*, 2019, **9**, 10.
17 Z. Y. Duan, M. Y. Song, T. G. Li, S. L. Liu, X. J. Xu, R. G. Qin, C. H. He, Y. Wang, L. Q. Xu and M. J. Zhang, *RSC Adv.*, 2018, **8**, 31542–31554.
18 Y. Zheng, P. Zhang, H. R. Yue, G. Xiang, Z. X. Qian, H. T. Li, W. Jiang, B. Liang, S. O. Pehkonen and S. J. Yuan, *Colloids Surf., A*, 2016, **502**, 89–101.
19 M. Y. Kim and T. G. Lee, *Chemosphere*, 2019, **217**, 423–429.
20 I. Uoginte, G. Lujaniene and K. Mazeika, *J. Hazard. Mater.*, 2019, **369**, 226–235.
21 X. M. Liu, K. N. Song, W. Z. Liu, Y. C. Xiong, Y. Y. Xu, Z. Q. Shi, D. Y. Zhao and Z. Lin, *Environ. Sci.: Nano*, 2019, **6**, 467–477.
22 M. Anari-Anaraki and A. Nezamzadeh-Ejhieh, *J. Colloid Interface Sci.*, 2015, **440**, 272–281.
23 L. Giraldo, A. Erto and J. C. Moreno-Pirajan, *Adsorption*, 2013, **19**, 465–474.
24 M. Rajabi, B. Mohammadi, A. Asghari, B. Barfi and M. Behzad, *J. Ind. Eng. Chem.*, 2014, **20**, 3737–3743.
25 Y. A. Feng, J. L. Gong, G. M. Zeng, Q. Y. Niu, H. Y. Zhang, C. G. Niu, J. H. Deng and M. Yan, *Chem. Eng. J.*, 2010, **162**, 487–494.
26 A. Stafiej and K. Pyrzynska, *Sep. Purif. Technol.*, 2007, **58**, 49–52.
27 W. Fang, X. Y. Jiang, H. J. Luo and J. J. Geng, *Chemosphere*, 2018, **197**, 594–602.
28 J. Y. Liu, Y. Chen, T. L. Han, M. Y. Cheng, W. Zhang, J. W. Long and X. Q. Fu, *Chemosphere*, 2019, **214**, 738–742.
29 S. Q. Shi, J. K. Yang, S. Liang, M. Y. Li, Q. Gan, K. K. Xiao and J. P. Hu, *Sci. Total Environ.*, 2018, **628–629**, 499–508.
30 R. Quiroga-Flores, A. Noshad, R. Wallenberg and L. Onnby, *Environ. Technol.*, 2019, 1–12.

31 L. H. Zhu, L. L. Zhang and Y. J. Tang, *Polym. Polym. Compos.*, 2014, **22**, 417–422.
32 Y. H. Gad, *Radiat. Phys. Chem.*, 2008, **77**, 1101–1107.
33 B. C. Xu, H. L. Zheng, Y. J. Wang, Y. Y. An, K. Luo, C. Zhao and W. Y. Xiang, *Int. J. Biol. Macromol.*, 2018, **112**, 648–655.
34 D. Lee, H. Maeda, A. Obata, K. Inukai, K. Kato and T. Kasuga, *Adv. Mater. Sci. Eng.*, 2013, 169721.
35 Y. Yang, Q. Q. Liang, J. H. Li, Y. Zhuang, Y. H. He, B. Bai and X. Wang, *Nano Res.*, 2011, **4**, 882–890.
36 P. Tang, Q. Sun, Z. Suo, L. Zhao, H. Yang, X. Xiong, H. Pu, N. Gan and H. Li, *Chem. Eng. J.*, 2018, **344**, 514–523.
37 J. Liu, G. Liu and W. Liu, *Chem. Eng. J.*, 2014, **257**, 299–308.
38 Y. Tang, M. Li, C. Mu, J. Zhou and B. Shi, *Chemosphere*, 2019, **229**, 570–579.
39 A. Leudjo Taka, K. Pillay and X. Yangkou Mbianda, *Carbohydr. Polym.*, 2017, **159**, 94–107.
40 K. Manzoor, M. Ahmad, S. Ahmad and S. Ikram, *RSC Adv.*, 2019, **9**, 7890–7902.
41 F. P. Zhao, W. Z. Tang, D. B. Zhao, Y. Meng, D. L. Yin and M. Sillanpaa, *Journal of Water Process Engineering*, 2014, **4**, 47–57.
42 L. Mouni, L. Belkhiri, F. Zouggaghe and M. Tafer, *Desalin. Water Treat.*, 2014, **52**, 6412–6419.
43 M. Momcilovic, M. Purenovic, A. Bojic, A. Zarubica and M. Randelovic, *Desalination*, 2011, **276**, 53–59.
44 S. Zhang, F. Xu, Y. F. Wang, W. Z. Zhang, X. L. Peng and F. Pepe, *Chem. Eng. J.*, 2013, **234**, 33–42.
45 D. F. Enache, E. Vasile, C. M. Simonescu, D. Culita, E. Vasile, O. Oprea, A. M. Pandele, A. Razvan, F. Dumitru and G. Nechifor, *RSC Adv.*, 2018, **8**, 176–189.
46 A. Moradi, P. N. Moghadam, R. Hasanzadeh and M. Sillanpaa, *RSC Adv.*, 2017, **7**, 433–448.
47 P. Tang, Q. Sun, L. Zhao, Y. Tang, Y. Liu, H. Pu, N. Gan, Y. Liu and H. Li, *Chem. Eng. J.*, 2019, **366**, 598–607.